An electrically excited nanoscale light source with active angular control of the emitted light

Eric Le Moal, Sylvie Marguet, Benoît Rogez, Samik Mukherjee, Philippe dos Santos, E. Boer-Duchemin, Geneviève Comtet, Gérald Dujardin

An electrically excited nanoscale light source with active angular control of the emitted light

Eric Le Moal,[*,†] *Sylvie Marguet,*[‡] *Benoît Rogez,*[†] *Samik Mukherjee,*[†,§] *Philippe Dos Santos,*[$] *Elizabeth Boer-Duchemin,*[†] *Geneviève Comtet,*[†] *Gérald Dujardin*[†]

[†]Institut des Sciences Moléculaires d'Orsay, CNRS – Université Paris-Sud (UMR 8214), Orsay, France

[‡]CNRS, IRAMIS, SPAM, Laboratoire Francis Perrin, URA 2453, Gif-sur-Yvette, France

[$]Fédération Lumière Matière (LUMAT FR2764), Orsay, France

Scanning tunneling microscopy, localized surface plasmon, inelastic electron tunneling, gold nanotriangle, truncated tetrahedron, photon nanosource.

We report on the angular distribution, polarization and spectrum of the light emitted from an electrically controlled nanoscale light source. This nanosource of light arises from the local, low-energy, electrical excitation of localized surface plasmons (LSP) on individual gold nanoparticles using a scanning tunneling microscope (STM). The gold nanoparticles (NP) are chemically synthesized truncated bitetrahedrons. The emitted light is collected through the transparent substrate and the emission characteristics (angular distribution, polarization and spectrum) are analyzed. These three observables are found to strongly depend on the lateral position of the

STM tip with respect to the triangular upper face of the gold NP. In particular, the resulting light emission changes orientation when the electrical excitation via the STM tip is moved from the base to the vertex of the triangular face. Based on the comparison of the experimental observations with an analytical dipole model and finite-difference time-domain (FDTD) calculations, we show that this behavior is linked to the selective excitation of the out-of-plane and in-plane dipolar LSP modes of the NP. This selective excitation is achieved through the lateral position of the tip with respect to the symmetry center of the NP.

Nanoscale light sources with controllable angular emission are highly desirable for future technological developments in nanophotonics. Many different concepts for directional photon nanosources have been proposed; most of them exploit the plasmonic modes of metallic nanostructures that are commonly called optical antennas.[1-6] In general, the principle of optical antennas for emission is the conversion of spatially confined, evanescent electromagnetic (EM) field into free propagating radiation.[7,8] One way to drive these optical antennas is to couple the near-field emission of a single fluorescent molecule[9-13] or nanocrystal[14-16] to the plasmonic modes of metallic nanostructures. This requires that the emitter be excited with photons from the far field, which gives rise to a strong excitation light background, thus limiting the possible integration with miniaturized devices. Moreover, except for a few cases where the emission directivity can be tailored through the polarization of the excitation light[17,18] or its incidence angle,[19] these *optically driven* photon nanosources only allow passive control of the radiation pattern; namely, their design must be modified in order to obtain a different result.

Alternatively, Coenen *et al* [20] have shown that directional light emission may be obtained from similar optical antennas by directly exciting their plasmonic modes with a high-energy electron beam (> 30 keV) focused to subwavelength dimensions (10 nm). In this case, the excitation is

extremely local and the electron-matter interaction itself generates, through a cathodoluminescence process,[21] the necessary localized evanescent EM field to feed the optical antenna.[22-29] Furthermore, active control of the emission pattern is made possible in this case by the spatially selective excitation of the different modes of the antenna with the tightly focused, scanning electron beam.[20,30,31] Nevertheless, a drawback of this approach is that it requires ultrahigh vacuum, high-voltage electron acceleration and magnetic lenses (i.e. the environment of a scanning electron microscope) to tightly focus the high-energy beam. The transfer of such a system to on-chip nanotechnological applications in the immediate future appears difficult. A low energy system working in air would be desirable.

In this Letter, we electrically excite localized surface plasmons with low-energy electrons (< 3 eV) tunneling from a sharp tungsten tip to a single gold nanoparticle (NP) of well-adapted shape to produce a nanoscale light source with active angular control of the emitted light. This concept uses the low energy electrons of a tunnel junction, works in an ambient environment, and may be adapted to a planar geometry. Using tunneling electrons guarantees the very high spatial selectivity of the electrical excitation. In our case, the tunnel junction is formed between the tip of a scanning tunneling microscope (STM) and the sample. The STM is also used to image the gold NP and locate the appropriate excitation sites.

It has long been known that inelastic electron tunneling between a metallic tip and a metallic sample generates light from the tunnel junction.[32-34] More precisely, tunneling electrons can couple to extremely localized plasmonic modes inside the tunnel junction (the so-called tip-induced gap plasmons), which originate from the tip-sample interaction and may in turn radiatively decay.[35-37] However, it is only very recently that these plasmons in the tunnel junction have been used as a nanoscale source of evanescent EM field to excite the propagating surface plasmons (SPP) of a nanostructured sample.[38-40] This excitation method produces a plasmonic

probe with very high spatial selectivity due to the lateral confinement of the tip-induced gap plasmons (less than 10 nm,[36,41] see details in the SI). Moreover, the resonance of these plasmons (which mainly depends on the tip and sample composition) is especially broad in frequency.[36] This is an important advantage for the efficient excitation of *localized* surface plasmons of different energies in a metallic nanostructure below the STM tip. Though earlier surface science studies have been dedicated to STM-induced light emission from metal clusters,[42-49] very few of them so far have been related to a single, well-defined metal NP.[50]

In this work, we investigate the mechanisms of localized surface plasmon excitation on a single gold NP using an STM. We show that this electrical excitation method provides a means of controlling the emission pattern by tuning the lateral position of the STM tip above the NP. We report on the first observation of the resulting emission pattern and its dependence on the tip position. Moreover, we find that the polarization distribution of the emission pattern is similar to that of a point dipole emitter whose orientation is gradually tilted when moving the STM tip off the NP center. The influence of the tip position on the *spectral* distribution of this STM-induced light emission is also studied. These experimental observations are interpreted on the basis of both a simple analytical dipole model and numerical finite-difference time-domain (FDTD) calculations. In this way, we show that part of the influence of the tip position is related to the selective excitation of the in-plane and out-of-plane dipolar LSP modes of the gold NP (with respect to the substrate plane).

The present study was possible due to the capabilities of the setup recently proposed by Wang *et al*,[51] which is depicted in Figure 1a. Briefly, an STM head operating in air is mounted on top of an inverted optical microscope. Inelastic electron tunneling from the STM tip to the sample induces photon emission, which is collected through the transparent substrate using an oil-immersion objective lens of numerical aperture NA = 1.45. An image of the back focal plane of

the objective lens (Fourier image) is recorded using a cooled charge-coupled device (CCD) camera, giving access to the polar and azimuthal distribution of the emitted light (angular emission pattern). A standard real-plane image may be obtained by simply removing a lens in the setup, in a similar manner as previously proposed by Egusa *et al*.[52] Alternatively, the collected light may be coupled to an optical fiber leading to an imaging spectrometer equipped with a nitrogen-cooled CCD camera, so as to measure the spectral distribution. We use electrochemically etched tungsten tips that are characterized using scanning electron microscopy (SEM) after all experiments are completed (radius of curvature estimated at 30 nm, see SEM images in the SI). All STM images and all optical images of STM-induced light emission are obtained with a sample bias of U_b = 2.75 V and setpoint current of I_t = 60 pA.

Truncated bitetrahedral gold NPs are obtained by colloidal chemistry in an aqueous solution using cetyltrimethylammonium bromide (CTAB) as the capping agent (see SI for details). A diluted solution of these NPs is deposited by droplet evaporation on a glass coverslip coated with a conductive, optically thin (100 nm) indium-tin oxide (ITO) layer. Individual NPs separated by more than 1 μm are obtained, allowing easy optical separation and avoiding plasmon coupling between NPs. Figure 1 shows an SEM image of a NP on ITO (Fig. 1b), together with a schematic top view defining its geometrical characteristics (Fig. 1c). Note that their side faces are not right-angled. Statistics on 60 NPs in SEM images indicated mean lengths of 81 ± 13 nm and 128 ± 6 nm for the upper and lower edges, respectively. Side views of the NPs (see SEM images in the SI) revealed a mean thickness of 69 ± 7 nm. We chose to study these NPs rather than more common, flat, right-angle triangular gold nanoprisms because of their lower aspect ratio (≈ 2) which yields dipolar plasmonic modes with resonance in the visible range. Figure 1 also shows a STM image of a NP on ITO (Fig. 1d). The high aspect ratio of the sharp STM tip allows the in-plane orientation of the NPs to be determined from the STM image to better than ±5°. However,

convolution with the STM tip shape hampers the imaging, and the edges of their upper face of the NP are indistinguishable; therefore we relied on the mean edge lengths determined from the abovementioned SEM studies to describe the NPs.

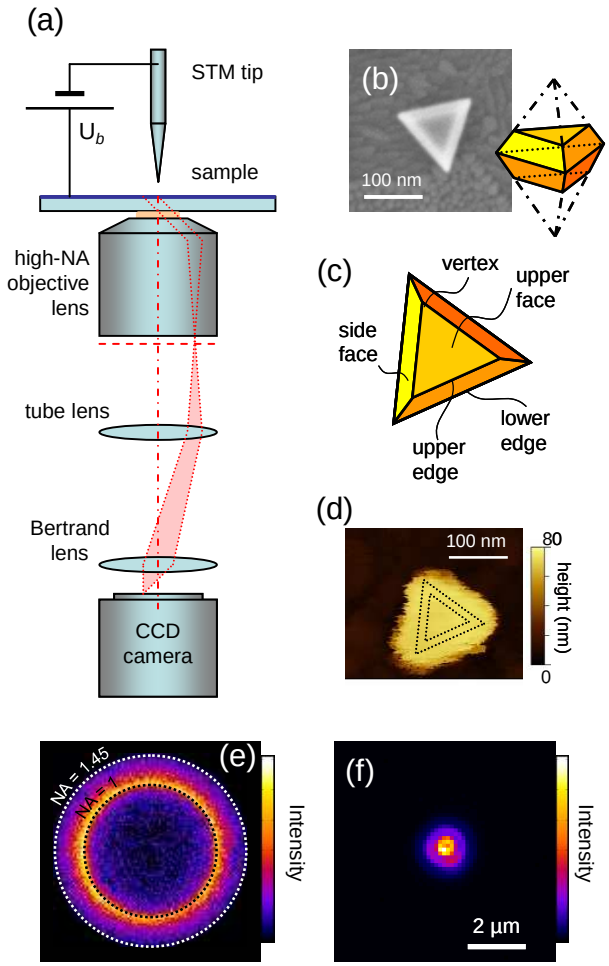

Figure 1. Experimental setup, truncated bitetrahedral gold nanoparticles (NPs) and optical images of the STM-induced photon emission. (a) Schematic of the setup consisting of a scanning tunneling microscope (STM) mounted on an inverted optical microscope. The sample consists of NPs on an ITO-coated glass slide, which is biased while the STM tip is grounded. Light emission from the sample is collected using an oil-immersion objective lens of high numerical aperture (NA) and focused on a cooled CCD camera using two lenses (the tube and Bertrand lenses) so as

to image the light pattern that forms in the back focal plane of the objective lens (Fourier image). Removing the Bertrand lens allows recording a standard real-plane image. (b) Top view SEM image with magnification of 97,590× giving a top view of the NP and, in inset, a schematic showing its truncated bitetrahedral shape. (c) Schematic top view of a NP showing the definitions used for its geometrical characteristics. (d) STM image of a NP, superimposed with equilateral triangles (dotted line) indicating NP's mean dimensions (mean edge length taken from SEM statistics, see text). (e) False-color CCD-camera Fourier image showing the angular emission pattern and (f) the associated real-plane image showing the spatial distribution of the emitted light from an STM-excited NP. In both cases, the STM excitation is above the center of the NP. In the Fourier image, the center is associated with emission along the optical axis (polar angle $\theta = 0$) while the circles labeled NA = 1 and NA = 1.45 (black and white dotted lines) show the critical angle of the air/glass interface ($\theta_c = 41°$ for $n_{glass} = 1.52$) and the maximum acceptance angle of the objective lens ($\theta_{max} = 72°$ for $n_{glass} = 1.52$), respectively.

Figure 1 shows the distribution of the emitted light after electrical excitation of a single NP with the STM tip above the center of the particle. The Fourier image (Fig. 1e) and real-plane image (Fig. 1f) are obtained under the same conditions. Both images are rotationally symmetric with respect to the optical axis. The Fourier image shows that the emitted light is equally distributed with respect to the azimuthal angle φ and that it is mainly emitted above the polar angle θ_c, the air/glass critical angle. The doughnut-shape in the real-space image, with its local intensity minimum at the center, is the signature of *p*-polarized emission typical of a vertical radiating dipole.[53]

Figure 2 shows how the angular emission pattern varies as the STM tip is moved with respect to the NP. Figure 2a is an STM image of the NP and the different positions along one of the three medians of its triangular face where the measurements are acquired. As illustrated in Fig. 2b, we position the STM tip at a specific location above the NP and obtain a Fourier image from which we retrieve a polar angle distribution of the emitted light. The results for the four different tip-particle positions noted in Fig. 2a are obtained under similar conditions (same STM parameters, same CCD camera settings, same STM tip), and are shown in Fig. 2c. As seen in Fig. 2d, we compare the experimental Fourier images and angular distributions to the emission pattern of a point dipole on an air/glass interface (in absence of tip and NP). The polar Θ and azimuthal Φ angles are fitting parameters defining the dipole orientation.[53] Though a dipole on an air glass/interface is a significant simplification of the system, the results of this simple model are similar to the experimental data, thus aiding in their interpretation. (A more realistic model including the tip and the nanoparticle is introduced later in the paper). Figure 2f shows the experimental (filled black curve) and corresponding simulated polar angle distributions (red line) along the direction of the median (see white dotted line in Fig. 2c). A red arrow represents the orientation of the dipole in the model.

Comparing Fig. 2c to Fig. 1e we see that the angular emission pattern loses its rotational symmetry and becomes asymmetric as the tip is moved away from the center of the NP. The emission pattern is anisotropic and this anisotropy changes when the tip is moved from close to the edge (base) to close to the vertex of the triangular upper face. In Figs. 2c and 2e, we see that the experimental Fourier images fit best with the emission pattern of a dipole that is not vertical but tilted (in the plane that is defined by the vertical axis and the median of the NP) when the tip is not above the center of the NP. Moreover, this tilt gradually varies as the tip moves from the vertex to the edge. The tilt of the dipole changes direction, while remaining in the

median/vertical axis plane, close to the NP center (an untilted dipole best fits the data of Fig. 1e). We conduct this experiment with the same tip on several NPs of different in-plane orientations and find the same tilts with relative reproducibility (to 10°). In particular, at the NP edge we find a tilted dipole with orientation $\Theta = 45°$, $\Phi = \Phi_{0;}$ an untilted dipole at the center ($\Theta = 0°$); and a dipole tilted in the opposite direction at the vertex ($\Theta = 30°$, $\Phi = \Phi_0 + 180°$). Φ_0 corresponds to the orientation of the median. From these results we see that the angular emission from an STM-excited NP is comparable to that of a tilted dipole on the substrate. We note from Fig. 2f, however, that the emitted light is even more concentrated in a particular direction than that from the best-fit tilted dipole. This discrepancy is very likely due to the oversimplification of the problem in this simple dipole model.

From Fig. 2c, we estimate the STM-induced photon emission efficiency or, more precisely, the statistical probability that a photon is emitted in the spectral range and solid angle of detection when one electron crosses the tunnel junction (see method in the SI). We find that this probability varies with tip position from less than 10^{-6} at the nanoparticle center to about 10^{-5} at the most off-centered position above the nanoparticle vertex.

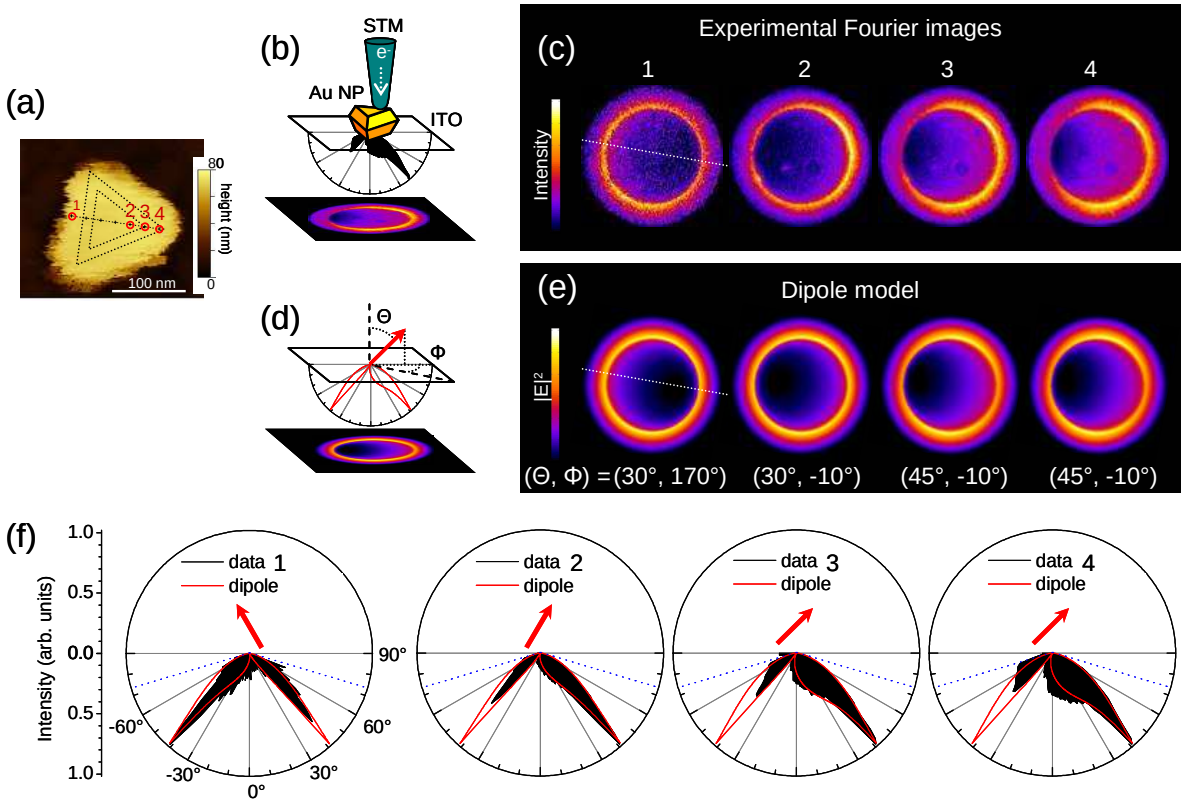

Figure 2. Influence of the tip position on the angular distribution of the STM-induced photon emission. (a) STM image of the NP (overlay: tip positions (numbered 1 to 4) along the median for which Fourier images are provided in Fig. 2c). On the STM image, the dashed edge contour represents the statistical mean edge-lengths previously determined from SEM images. (b) Schematics of the experimental configuration with the STM tip above the NP on the ITO-coated substrate; the Fourier image is a projection of the angular emission pattern; intensity profiles along a cross-section of the Fourier image may be plotted in a polar graph, thus providing the distribution of the emission intensity versus polar angle θ. (c) False-color experimental Fourier images obtained with the STM tip at positions 1 to 4 of Fig. 2a. (d) Graphic representation of the simple analytical model that is used to interpret the experimental results: the Fourier images and the angular distribution of the emitted light are compared to those of a point dipole emitter located on an air-glass interface, with the dipole orientation defined by the azimuthal Φ and polar

Θ angles with respect to horizontal (median) and vertical (optical) axes, respectively. (e) Theoretical Fourier images calculated with this simple model. The appropriate polar dipole orientation angle Θ is determined by calculating different theoretical images while varying Θ in steps of 5° until the best theoretical image with respect to the experimental Fourier image is found. Φ is chosen so that the dipole has same azimuthal orientation as the median of the NP's triangular face. (f) Polar plot of the intensity versus polar angle θ, obtained from the intensity profiles along the median (dotted line in Fourier image) on both the experimental (filled curve) and theoretical (red line) Fourier images. Dotted lines at $\theta_{max} = \pm 72°$ help visualize the collection cone of the objective lens. For the experimental images a shortpass filter (cut-off wavelength 842 nm or 1.47 eV) is placed in front of the CCD camera.

Figure 3 shows the distribution of the emitted light in Fourier space as a function of STM tip position when a linear polarizer is placed between the objective and tube lenses. The goal of this experiment is to confirm the hypothesis that the light emission from the NP upon STM excitation is comparable, to a first approximation, to the radiation of a point dipole emitter whose orientation depends on the STM tip position. Figure 3a shows the tip locations along a median of the NP's triangular face. The experimental and simulated polarization-filtered Fourier images with the best dipole orientation fitting parameters (Θ,Φ) are found in Fig. 3b and c. For a vertical radiating dipole (Θ = 0), *p*-polarized emission is expected. The intensity of such emission is invariant as a function of the azimuthal angle φ and appears radially polarized in the Fourier plane (similar to Fig. 1e). Therefore the emission intensity with a polarizer oriented along the *x*-axis is expected to follow a $cos^2\varphi$ law, with intensity minima along the *y*-axis. Figure 3b-3 shows that this $cos^2\varphi$ law is indeed verified experimentally when the STM tip is located above the

center of the NP. However, as soon as the tip is moved away from the center of the NP, this behavior is no longer observed. In the cases where the tip is off-center, the polarization-filtered Fourier images are best fit by the theoretical polarization distribution of a *tilted* dipole. The polarization-filtered measurements confirm that this tilt gradually varies as the STM tip moves from vertex to edge and changes direction, while remaining in the median/vertical axis plane when passing through the NP center. We carry out the same experiment on a differently oriented NP and find that the polarization of the light emission solely depends on the relative position of the tip with respect to the NP, thus excluding any artifacts from a possible asymmetry of the tip.

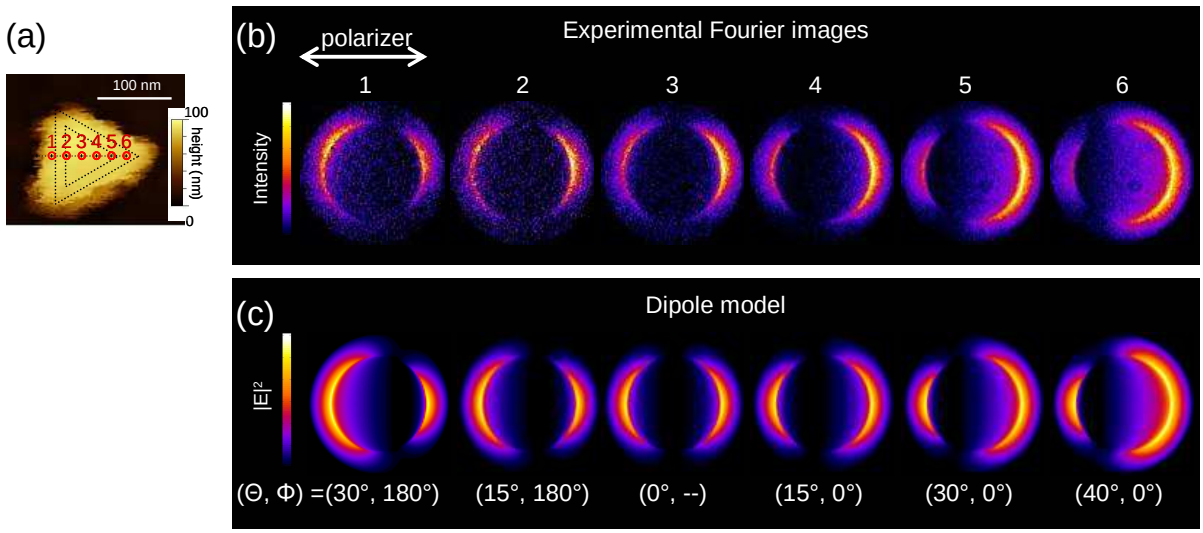

Figure 3. Influence of the STM tip position on the polarization distribution of the STM-induced light. (a) STM image of the NP (overlay: tip positions for data collection). (b) False-color polarization-filtered Fourier images obtained with the STM tip at six different positions along the median of the triangular upper face of the NP. A linear polarizer is placed between the objective and tube lenses. The polarizer axis is oriented as indicated by the white arrow. (c) Theoretical polarization-filtered Fourier images calculated for a dipole on an air/glass interface with the best fitting polar (Θ) orientation parameter. The azimuthal (Φ) orientation is chosen such that the

dipole is in the median/vertical axis plane. The presence of the linear polarizer is taken into account in the model by displaying the squared modulus of the electric field component along the transmission axis of the polarizer ($|E_x|^2$) at each point in the image. For the experimental images a shortpass filter (cut-off wavelength 842 nm or 1.47 eV) is placed in front of the CCD camera.

Spectral analysis of STM-induced light can provide a better understanding of the electromagnetic coupling between the STM tip and the sample.[54] We spectrally analyze the light emitted from the STM excitation of a NP for two typical cases: in one case the tip is located above a vertex of the NP (Fig. 4a) and in the other the tip is located above the NP's center (Fig. 4b).

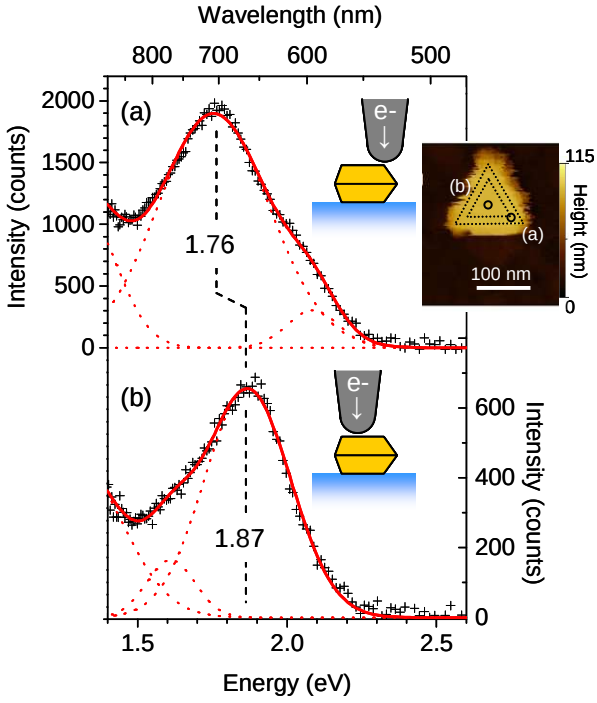

Figure 4. Spectral distribution of the STM-induced light from a single NP for two different tip excitation positions. The inset is an STM image of the NP (two equilateral triangles indicate the

upper and lower edges, as determined from the statistical analysis of SEM images). As marked on the STM image (black circles), the STM tip is located either (a) above the vertex of the NP or (b) above its center. The intensity (exposure time 30 s) has been corrected for the transmission of the optics (objective lens, tube lens, mirrors, and optical fiber), the diffraction efficiency of the grating in the spectrometer and the quantum efficiency of the CCD camera. In (a) and (b), the experimental data (crosses) have been fitted with a series of Gaussian peaks (dashed lines: individual peaks, straight line: sum of the peaks).

The STM-induced light exhibits a relatively broad spectrum that is dominated by a peak at 1.76 eV when the tip is located above the vertex of the NP (Fig. 4a) and by a peak at 1.87 eV when the tip is above the NP's center (Fig. 4b). With the tip at the vertex position, a secondary contribution may also be observed at 2.09 eV. Other contributions may also exist farther in the near infrared (NIR) but their energies are not detectable with our setup. This is taken into account in Fig. 4 by fitting the lower energy part of the spectra with the tail of a Gaussian curve centered at 1.3 eV. Nevertheless, these NIR components do not contribute to the Fourier images shown in Figs. 2 and 3 as a shortpass filter (cut-off wavelength 842 nm or 1.47 eV) was placed in front of the CCD camera.

The dominant peaks in Figs. 4a and 4b are broadened and slightly shifted in energy compared to the resonances of the dipolar LSP modes of the NP as determined by optical spectroscopy in absence of the STM tip (see the light scattering spectra in the SI). Larger resonance shifts (by 0.6 eV) have been previously reported by Freund *et al* [50] for silver NPs, 4 nm in diameter, excited by STM with a silver tip. This result may be explained by the much lower losses in silver as compared to tungsten in the visible. The plasmon modes of the tungsten tip are indeed strongly

damped in the visible range (the dielectric function of tungsten has a large imaginary component).[54] Changing the tip location on the NP may also influence the LSP resonance by modifying the local dielectric environment of the NP, which may play a part in the spectral variations seen in Fig. 4. However, the fact that both the spectral distribution and the polarization of the STM-induced light vary as a function of the excitation site suggests that the STM tip excites two different LSP modes of the NP.

Variation of the spectral response with the lateral position of the tip has also been reported by Umeno *et al* [44] in the case of nearly spherical gold NPs of diameter 10 – 20 nm excited with an asymmetric tungsten tip. The authors ascribe this spectral shift to the influence of the radius of curvature of the tip on the tip-induced gap plasmons, which obviously changes when an asymmetric tip is moved from one side of a nanosphere to the other. In our case, the STM tip is highly symmetrical (see SEM images in the SI). Moreover, we observe reproducibly the same behavior and same energy shift on other NPs that are excited with the same tip, whatever the in-plane orientation of the NPs. Thus, tip asymmetry is excluded as the origin of the observed phenomenon, giving support to the idea that this dependence is related to the NP LSP modes. Given their aspect ratio (NP thickness is about half the edge length), the resonance of the in-plane dipolar LSP mode of our NPs is expected to be at a lower energy than that of the out-of-plane dipolar LSP mode of the particles.[55] This observation, together with the polarization measurements, leads to the conclusion that the STM tip efficiently excites both the in-plane (horizontally polarized) and out-of-plane (vertically polarized) dipolar LSP of the NP when it stands above the vertex, leading to the equivalent of a tilted dipole, whereas the out-of-plane (vertically polarized) dipolar LSP dominates when the tip is centered (only this mode is compatible with *p*-polarized emission). In the following, thanks to time-dependent numerical

calculations, we propose an explanation of the mechanisms behind this selective excitation of the NP modes.

In order to investigate the electromagnetic response of our system, we conduct FDTD calculations using a freely available software package (Meep).[56] Briefly, we define a three-dimensional computational domain including the tungsten tip, the gold NP, the surrounding air and the glass substrate (see details in the SI). To model the tip-induced gap plasmon, we consider a point dipole source located in the STM junction, equidistant between the closest points of the tip and the NP. In order to get an idea of the system behavior at resonance, we choose a monochromatic source and wait for the steady-state electromagnetic field to fully evolve before analyzing the results. The oscillation frequency of the source corresponds to the average of the two dipolar LSP resonances of the NP as determined from Fig. 4 (1.81 eV).

Moving the tip off the NP center breaks the rotational symmetry of the tip-NP system, which may drastically modify the coupling between the tip-induced gap plasmon and the NP modes. This is one possible explanation for our experimental observations. Another involves the fact that at the most off-centered tip positions, the electron tunneling may occur between the tip and the upper edge or the side face of the NP. In this case the effective STM junction is tilted and the tip-induced gap plasmon should not be described as a vertical dipole as in the case of a vertical STM junction,[36] but as a dipole tilted by the same angle. This tilt might also modify the coupling efficiency between the tip-induced gap plasmon and the different LSP modes of the NP. In order to distinguish between these possible explanations, we first consider a case where a tilted STM junction cannot occur. Namely, we simplify the truncated bitetrahedral shape of the NP with that of a triangular nanoprism, with upper and lower triangular faces of the same size and vertical rectangular side faces (see sketch in the inset of Fig. 5a). Numerically we then consider tip

positions where electron tunneling occurs between the bottom of the tip and the horizontal upper face (i.e. the tip-induced gap plasmon can be modeled as a vertical dipole).

Figures 5b to 5f show the *near field* distribution of the time-averaged electric field energy density ($\frac{1}{2}\varepsilon|E|^2$ where ε is the permittivity and $|E|^2$ the squared modulus of the electric field, averaged over one oscillation period), calculated for several tip positions using the FDTD program. The asymmetry of the electric field distribution in the substrate becomes increasingly pronounced as the tip is laterally moved away from the NP center. For comparison purposes, the time-averaged electric near field energy density has also been computed for an electric dipole on the air-glass interface, in the absence of the tip and NP (see Fig. 5g). The dipole orientation in Figs. 5h to 5l is chosen in order to best fit the results of the FDTD calculation in Figs. 5b to 5f. This comparison shows that the electric near field distribution obtained for an off-centered tip above a NP is very similar to that of a tilted electric dipole. The tilt of this effective dipole follows the same trends as previously deduced from the *farfield* emission patterns in Figs. 2 and 3 (i.e. the tilt gradually varies as the tip moves from the vertex to edge and changes direction, close to the NP center, while remaining in the median/vertical axis plane). Since the actual point dipole source in the FDTD model is always vertical, the results in Fig. 5 show that the control of the emission pattern via the tip position does *not* require a change in the orientation of the tip-induced gap plasmon. Consequently, such control can also be exerted on a NP that does not have tilted side faces.

In addition, we also carry out the same calculations as in Figs. 5b to 5f, but without the tip. This is equivalent to moving a vertical electric dipole above the horizontal upper face of the NP; remarkably, the results (not shown here) are qualitatively similar to those in Fig. 5, with the same reshaping of the electric near field distribution in the substrate when the dipole is moved away from the NP center. Finally, we repeat the calculations of Figs. 5b to 5f with the NP modeled as a

truncated tetrahedron and the results are again very similar (see the SI); namely, we find that the electric nearfield distribution in the substrate becomes increasingly asymmetric as the tip is laterally moved away from the NP center. The main difference when taking into account the tilted side faces of the NP in the model is that this asymmetry is slightly more pronounced for the most off-centered tip positions, i.e. when electron tunneling can occur between the tip and the tilted side face of the NP. All together, these observations show that the excitation site is the most important parameter for the control of the emission pattern.

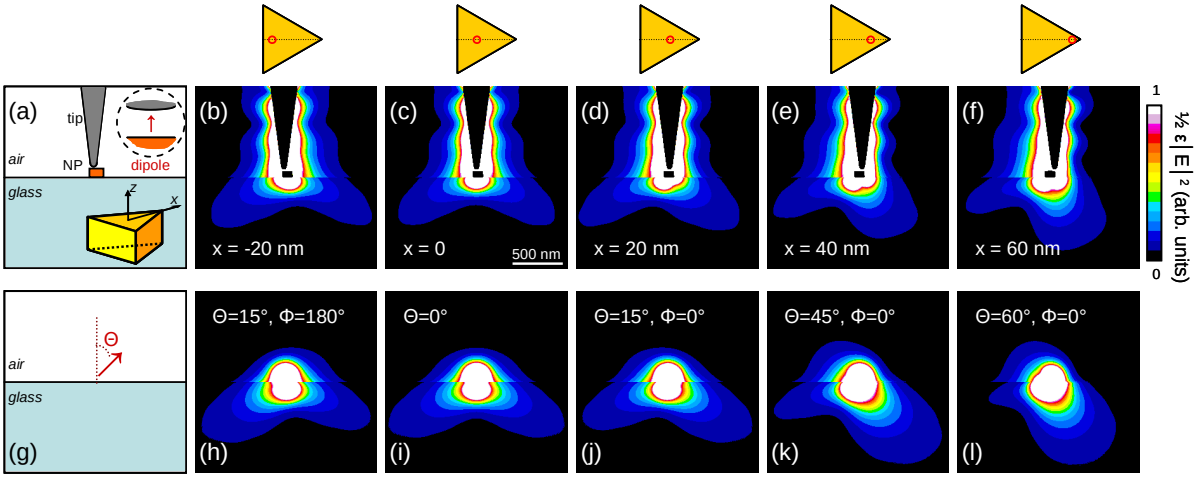

Figure 5. FDTD calculations of the steady state, time-averaged electric near field energy density in the *xz* plane for (a-f) a vertical electric dipole in the gap between a tungsten tip and a gold NP in air on a glass substrate and (g-l) an electric dipole of various orientations in the *xz* plane on an air/glass interface. In this model, the NP shape is a triangular gold nanoprism of edge-length 130 nm and thickness 65 nm (see the sketch in the inset to Fig. 5a). In (b-f), the tip and vertical dipole representing the tip-induced gap plasmon are located at different positions: *x* varies from -20 nm to 60 nm along the *x* axis (median of the triangular upper face of the gold nanoprism) where "*x* = 0" is above the center of the NP. In (h-l), the dipole orientation is defined by the angle Θ as shown in (g). This angle is determined from the best fit with the results in (b-f),

in terms of electric field distribution in the substrate. In (a-l), the dipole oscillates at a frequency corresponding to an energy of 1.81 eV (wavelength 685 nm in vacuum).

In order to further clarify this phenomenon, we obtain the vector components of the electric field along the horizontal *x* (E_x) and vertical *z* (E_z) axes from our FDTD calculations, for the same system as in Fig. 5a. As shown in Figure 6, we consider two tip locations: one above the NP center (a,b) and the other above the vertex (d,e). In each case, a snapshot of the electric field at a given time is displayed. The red and blue of the color scale denote field amplitudes of opposite sign. Interestingly, we see in Fig. 6a that the horizontal components of the electric field are *out of phase* on opposite sides of the NP, while in Fig. 6b the vertical components of the electric field are *in phase* on the upper and lower faces of the NP. This result is not surprising since the rotational symmetry of the system assures that the horizontal components of the electric field cancel out on average. This outcome, with the zero averaged horizontal field and in-phase vertical electric field, shows that the nearfield of the vertical electric dipole (tip-induced gap plasmon) can vertically polarize the NP when the tip is centered, as illustrated in Fig. 6c.

The result when the tip is at its most off-centered position is very different; the horizontal components of the electric field are *in phase* on opposite sides of the NP (see Fig. 6d), while its vertical components are *out of phase* on the upper and lower faces (see Fig. 6e). Thus, the vertical electric dipole nearfield mainly polarizes the NP along its horizontal axis (see Fig. 6f). Hence we conclude that the tip-induced gap plasmon between the tip and NP can selectively excite either the out-of-plane or in-plane dipolar LSP modes of the NP depending on where on the NP the STM excitation takes place. Control of this selective excitation is possible via the accurate positioning of the STM tip above the NP.

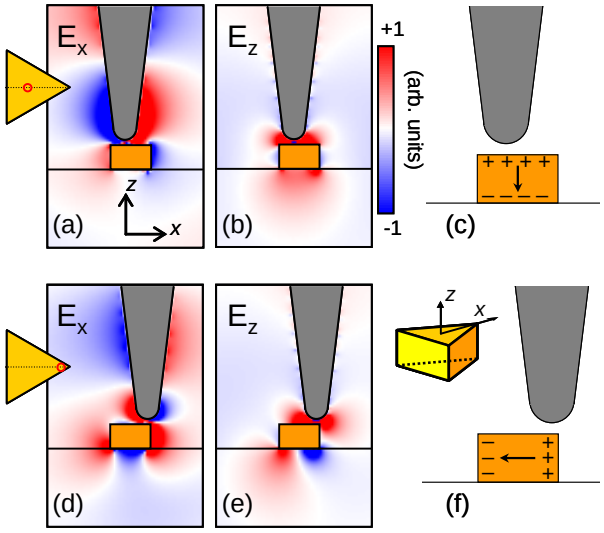

Figure 6. FDTD calculations of the electric field components E_x (a,d) and E_z (b,e) at a given time in the *xz* plane for the same system as in Fig. 5a. The tip and the vertical dipole are located at either (a,b) $x = 0$, right above the center of the NP, or (d,e) laterally shifted to $x = 60$ nm, above the vertex of the NP. The *red* and *blue* color scale corresponds to field amplitudes of opposite sign, while *white* represents zero amplitude. Schematics (c) and (f) depict the charge displacement at a given time, as deduced from (a,b) and (d,e) respectively, as well as the corresponding polarization of the NP.

In summary, we show that the lateral position of the STM tip above the NP strongly influences the angular distribution, polarization and spectrum of the STM-induced light in a deterministic way. Repeating these experiments on several NPs of random in-plane orientation eliminates the possibility of artifacts arising from the tip shape. The influence of the tip position on the angular distribution and polarization is clarified using FDTD calculations. We model the tip-induced gap plasmon as a vertical electric dipole and we show that moving this vertical dipole to an off-center position on the NP yields an electric field energy density distribution resembling that of a tilted dipole (i.e., arising from the in-plane and out-of-plane LSP modes of the particle). The same

effect is qualitatively found from the FDTD calculations, no matter what type of side faces (tilted or right-angled) the NP has; thus we presume that this effect is general and does not require tilted faces. We also calculate the electric field components in the nearfield of the NP and find that the vertical dipole can horizontally polarize the NP provided that it is off-centered. In brief, the tip-induced gap plasmon in the STM junction can selectively couple to the out-of-plane and in-plane dipolar LSP modes of the NP depending on the lateral position of the tip with respect to the center of the NP. As the tip is moved further away from the center of the NP, the relative contribution of the in-plane LSP mode increases and the resulting angular emission distribution in the far field becomes more asymmetric. All together, our observations indicate that this asymmetric angular distribution occurs as soon as the tip is off-centered and does not require that electrons tunnel from the tip to the side faces of the NP.

In conclusion, inelastic electron tunneling between a sharp tungsten tip and a single gold nanostructure of tailored shape provides a promising way to activate directional light emission from a nanoscale source. Continuous control of the angular emission pattern is possible by finely tuning the tip position with respect to the nanostructure. It is quite likely that NPs of different symmetry orders or a more anisotropic shape than those used here could yield even more pronounced directional effects. Our low-energy electrical excitation method of actuating photon nanosources has many advantages over excitation with photons or high-energy electrons in a context of nanodevice applications. Spatial selectivity far beyond the diffraction limit is guaranteed by the strong confinement of the tip-induced gap plasmon. Moreover, inducing light emission by inelastic electron tunneling is possible in air with junction biases lower than 3 V, making it fully compatible with break-junction geometries,[57,58] and in-plane or stacked electrodes.[59]

ASSOCIATED CONTENT

Supporting Information. Further discussion on the spatial confinement of tip-induced gap plasmons; methods for NP synthesis and characterization; STM tip characterization; estimation of STM-induced photon emission efficiency; dark-field spectra of individual NPs; methods and complementary results of FDTD calculations. This material is available free of charge via the Internet at http://pubs.acs.org.

AUTHOR INFORMATION

Corresponding Author

* (E. L. M.) Tel: +33 1 69 15 66 97. Fax: +33 1 69 15 67 77. E-mail: eric.le-moal@u-psud.fr.

Present Addresses

§S. Mukherjee is now at the Nano and Hybrid Materials Laboratory, École Polytechnique de Montréal, Québec, Canada.

Funding Sources

This work was supported by the ANR project NAPHO (contract ANR-08-NANO-054), the European STREP ARTIST (contract FP7 243421) and funding from Université Paris-Sud through grant “Attractivité 2013”.

Notes

The authors declare no competing financial interest.

ACKNOWLEDGMENT

We acknowledge technical support from the “Centrale de Technologie Universitaire IEF-Minerve” in Orsay. One of the authors (S. Marguet) thanks the Region Ile-de-France for financial support regarding SEM experiments. We acknowledge the use of the computing facility cluster GMPCS of the LUMAT federation (FR LUMAT 2764). The authors thank Andrei G. Borissov, Dana-Codruta Marinica and Georges Raseev for fruitful discussions.

REFERENCES

(1) Koenderink, A. F. Nano Lett., **2009**, *9*, 4228–4233.

(2) Bharadwaj, P.; Deutsch, B.; Novotny, L. Adv. Opt. Photon. **2009**, *1*, 438–483.

(3) Esteban, R.; Teperik, T.V.; Greffet, J. J. Phys. Rev. Lett. **2010**, *104*, 026802.

(4) Giannini, V.; Fernandez-Domínguez, A. I.; Heck, S. C.; Maier, S. A. Chem. Rev. **2011**, *111*, 3888–3912.

(5) Li, Z.; Hao, F.; Huang, Y.; Fang, Y.; Nordlander, P.; Xu, H. Nano Lett. **2009**, *9*, 4383–4386.

(6) Shegai, T.; Miljkovic, V. D.; Bao, K.; Xu, H.; Nordlander, P.; Johansson, P.; Käll, M. Nano Lett. **2011**, *11*, 706–711.

(7) Greffet, J.-J. Science **2005**, *308*, 1561–1563.

(8) Novotny, L.; van Hulst, N. Nat. Photon. **2011**, *5*, 83–90.

(9) Ahmed A.; Gordon, R. Nano Lett., **2011**, *11*, 1800–1803.

(10) Aouani, H.; Mahboub, O.; Bonod, N.; Devaux, E.; Popov, E.; Rigneault, H.; Ebbesen, T. W.; Wenger, J. Nano Lett., **2011**, *11*, 637–644.

(11) Aouani, H.; Mahboub, O.; Devaux, E.; Rigneault, H.; Ebbesen, T. W.; Wenger, J. Nano Lett., **2011**, *11*, 2400–2406.

(12) Zhu, W.; Wang, D.; Crozier, K. B. Nano Lett., **2012**, *12*, 6235–6243.

(13) Lu, G.; Li, W.; Zhang, T.; Yue, S.; Liu, J.; Hou, L.; Li, Z.; Gong, Q. ACS Nano, **2012**, *6*, 1438–1448.

(14) Taminiau, T. H., Stefani, F. D.; van Hulst, N. F. Opt. Express **2008**, *16*, 10858-10866.

(15) Curto, A. G.; Volpe, G.; Taminiau, T. H.; Kreuzer, M. P.; Quidant, R.; van Hulst, N. F. Science **2010**, *329*, 930–933.

(16) Belacel, C.; Habert, B.; Bigourdan, F.; Marquier, F.; Hugonin, J.-P.; Michaelis de Vasconcellos, S.; Lafosse, X.; Coolen, L.; Schwob, C.; Javaux, C.; Dubertret, B.; Greffet, J.-J.; Senellart, P.; Maitre, A. Nano Lett., **2013**, *13*, 1516–1521.

(17) Dregely, D.; Taubert, R.; Dorfmüller, J.; Vogelgesang, R.; Kern, K.; Giessen, H. Nat. Comm. **2011**, *2*, 267.

(18) Lal, S.; Hafner, J. H.; Halas, N. J.; Link, S.; Nordlander, P. Acc. Chem. Res. **2012**, *45*, 1887–1895.

(19) Munárriz, J.; Malyshev, A. V.; Malyshev, V. A.; Knoester, J. Nano Lett. **2013**, *13*, 444−450.

(20) Coenen, T.; Vesseur, E. J. R.; Polman, A.; Koenderink A. F. Nano Lett **2011**, *11*, 3779–3784.

(21) García de Abajo, F. J. Rev. Mod. Phys. **2010**, *82*, 209–274.

(22) Yamamoto, N.; Araya, K.; Garcia de Abajo, F. J. Phys. Rev. B **2001**, *64*, 205419

(23) Vesseur, E.J.R.; de Waele, R.; Kuttge, M.; Polman, A. Nano Lett. **2007**, *7*, 2843–2846.

(24) Gomez-Medina, R.; Yamamoto, N.; Garcia de Abajo, F. J.; New J. Phys. **2008**, *10*, 105009.

(25) Chaturvedi, P.; Hsu, K. H.; Kumar, A.; Fung, K. H.; Mabon, J. C.; Fang, N. X. ACS Nano **2009**, *3*, 2965–2974.

(26) Kumar, A.; Fung, K.-H.; Mabon, J. C.; Chow, E.; Fang, N. X. J. Vac. Sci. Technol., B **2010**, *28*, C6C21–C26C25.

(27) Edwards, P. R.; Sleith, D.; Wark, A. W.; Martin, R. W. J. Phys. Chem. C **2011**, *115*, 14031–14035.

(28) Myroshnychenko, V.; Nelayah, J.; Adamo, G.; Geuquet, N.; Rodríguez-Fernández, J.; Pastoriza-Santos, I.; MacDonald, K. F.; Henrard, Liz-Marzán, L. M.; Zheludev, N. I.; Kociak, M.; García de Abajo, F. J. Nano Lett. **2012**, *12*, 4172−4180.

(29) Knight, M. W.; Liu, L. Wang, Y.; Brown, L.; Mukherjee, S.; King, N. S.; Everitt, H. O.; Nordlander, P.; Halas N. J. Nano Lett., **2012**, *12*, 6000–6004.

(30) Coenen, T.; Vesseur, E. J. R.; Polman A. ACS Nano, **2012**, *6*, 1742–1750.

(31) Schoen, D. T.; Coenen, T.; García de Abajo, F. J.; Brongersma, M. L., Polman, A. Nano Lett., **2013**, *13*, 188–193.

(32) Lambe, J. Phys. Rev. Lett. **1976**, *37*, 923.

(33) Berndt, R.; Gimzewski, J. K.; Johansson, P.; Phys. Rev. Lett. **1991**, *67*, 3796.

(34) Takeuchi, K.; Uehara, Y.; Ushioda, S.; Morita, S. J. Vac. Sci. & Technol. B **1991**, *9*, 557.

(35) Uehara, Y.; Kimura, Y.; Ushioda, S.; Takeuchi, K. Jpn. J. Appl. Phys. **1992**, *31*, 2465–2469

(36) Johansson, P. Phys. Rev. B **1998**, *58*, 10823.

(37) Douillard, L.; Charra, F.; J. Phys. D: Appl. Phys. **2011**, *44*, 464002.

(38) Bharadwaj, P.; Bouhelier, A.; Novotny, L. Phys. Rev. Lett. **2011**, *106*, 226802.

(39) Wang, T. PhD dissertation, Université Paris-Sud (France), **2012**.

(40) Zhang, Y.; Boer-Duchemin, E.; Wang, T.; Rogez, B.; Comtet, G.; Le Moal, E.; Dujardin, G.; Hohenau, A.; Gruber, C.; Krenn, J. R. Optics Express **2013**, *21*, 13938–13948.

(41) Rendell, R. W.; Scalapino, D. J. Phys. Rev. B **1981**, *24*, 3276–3274.

(42) Venkateswaran, N.; Sattler, K.; Xhie, J.; Ge, M. Surf. Sci. **1992**, *274*, 199-204.

(43) Ito, K.; Ohyama, S.; Uehara, Y.; Ushioda, S. Surf. Sci. **1995**, *324*, 282-288.

(44) Umeno, T.; Nishitani, R.; Kasuya, A.; Nishina, Y. Phys. Rev. B **1996**, *54*, 13499.

(45) Bischoff, M.M.J.; van der Wielen, M.C.M.M.; van Kempen, H. Surf. Sci. **1998**, *400*, 127–133.

(46) Taleb, A.; Gusev, A.O.; Silly, F.; Charra, F.; Pileni, M.-P. Appl. Surf. Sci. **2000**, *162–163*, 553–558.

(47) Silly, F.; Gusev, A. O.; Taleb, A.; Pileni, M.-P.; Charra, F. Mater. Sci. Eng. C **2002**, *19*, 193–195.

(48) Arai, T.; Nakayama, K. Appl. Surf. Sci. **2005**, *246*, 193–198.

(49) Branscheid, R.; Jacobsen, V.; Kreiter, M. Surf. Sci. **2008**, *602*, 176–181.

(50) Myrach, P.; Nilius, N.; Freund, H.-J. Phys. Rev. B **2011**, 83, 035416.

(51) Wang, T.; Boer-Duchemin, E.; Zhang, Y.; Comtet, G.; Dujardin, G. Nanotechnology **2011**, *22*, 175201.

(52) Egusa, S.; Liau, Y.-H.; Scherer, N. F. Appl. Phys. Lett. **2004**, *84*, 1257–1259.

(53) Lieb, M. A.; Zavislan, J. M.; Novotny, L. J. Opt. Soc. Am. B **2004**, *21*, 1210–1215.

(54) Berndt, R.; Gimzewski, J. K.; Johansson, P. Phys. Rev. Lett. **1993**, *71*, 3493.

(55) Talebi, N., Sigle, W.; Vogelgesang, R.; Koch, C. T.; Fernández-López, C.; Liz-Marzán, L. M.; Ögüt, B.; Rohm, M.; van Aken, P. A. Langmuir **2012**, *28*, 8867−8873.

(56) Oskooi, A. F.; Roundy, D.; Ibanescu, M.; Bermel, P.; Joannopoulos, J. D.; Johnson, S. G. Computer Physics Communications **2010**, *181*, 687–702.

(57) Bolotin, K. I.; Kuemmeth, F.; Pasupathy, A. N.; Ralph, D. C. Appl. Phys. Lett. **2004**, *84*, 3154.

(58) Mangin, A.; Anthore, A.; Della Rocca, M. L.; Boulat, E.; Lafarge, P. J. Appl. Phys. **2009**, *105*, 014313.

(59) Huang, K. C. Y.; Seo, M.-K.; Huo, Y.; Sarmiento, T.; Harris, J. S.; Brongersma, M. L. Nat. Comm. **2012**, *3*, 1005.